Numerical investigation of turbulence in abdominal aortic aneurysms

Rawat, Digvijay S.; Pourquie, Mathieu; Poelma, Christian

DOI
10.1115/1.4043289

Publication date
2019

Document Version
Final published version

Published in
Journal of Biomechanical Engineering

Numerical Investigation of Turbulence in Abdominal Aortic Aneurysms

Digvijay S. Rawat
Laboratory for Aero & Hydrodynamics,
Delft University of Technology,
Leeghwaterstraat 21,
Delft CA 2628, The Netherlands
e-mail: D.S.Rawat@student.tudelft.nl

Mathieu Pourquie
Laboratory for Aero & Hydrodynamics,
Delft University of Technology,
Leeghwaterstraat 21,
Delft CA 2628, The Netherlands
e-mail: M.J.B.M.Pourquie@tudelft.nl

Christian Poelma[1]
Laboratory for Aero & Hydrodynamics,
Delft University of Technology,
Leeghwaterstraat 21,
Delft CA 2628, The Netherlands
e-mail: C.Poelma@tudelft.nl

Computational fluid dynamics (CFD) is a powerful method to investigate aneurysms. The primary focus of most investigations has been to compute various hemodynamic parameters to assess the risk posed by an aneurysm. Despite the occurrence of transitional flow in aneurysms, turbulence has not received much attention. In this article, we investigate turbulence in the context of abdominal aortic aneurysms (AAA). Since the clinical practice is to diagnose an AAA on the basis of its size, hypothetical axisymmetric geometries of various sizes are constructed. In general, just after the peak systole, a vortex ring is shed from the expansion region of an AAA. As the ring advects downstream, an azimuthal instability sets in and grows in amplitude thereby destabilizing the ring. The eventual breakdown of the vortex ring into smaller vortices leads to turbulent fluctuations. A residence time study is also done to identify blood recirculation zones, as a recirculation region can lead to degradation of the arterial wall. In some of the geometries simulated, the enhanced local mixing due to turbulence does not allow a recirculation zone to form, whereas in other geometries, turbulence had no effect on them. The location and consequence of a recirculation zone suggest that it could develop into an intraluminal thrombus (ILT). Finally, the possible impact of turbulence on the oscillatory shear index (OSI), a hemodynamic parameter, is explored. To conclude, this study highlights how a small change in the geometric aspects of an AAA can lead to a vastly different flow field.
[DOI: 10.1115/1.4043289]

Keywords: aneurysm, turbulence, computational fluid dynamics, pulsatile flow, vortex ring, recirculation region, oscillatory shear index

1 Introduction

An aneurysm refers to the localized dilation or bulging of a blood vessel. Aneurysms can form in any blood vessel, but the cerebral arterial system and the aorta are the most common locations for their formation. Further, aortic aneurysms can be located either in the thoracic region or in the abdominal region, the latter being commonly referred to as an abdominal aortic aneurysm (AAA). The majority of cases involving an AAA is asymptomatic and as such keep growing in size until they may eventually rupture. Rupture of an AAA results in massive internal bleeding, which more often than not leads to death [1]. Unfortunately, our understanding in relation to the inception, growth, and rupture of an aneurysm is still not very comprehensive [2,3]. The chief reason for this is the plethora of factors involved in the lifetime of an AAA, ranging from aorta degeneration to the variable hemodynamic forces experienced by the aortic wall. Hence, the current clinical practice to decide if an AAA needs surgical attention is chiefly decided by its diameter; surgery is usually done if the diameter exceeds 5.5 cm in men or 5 cm in women [4] despite the common knowledge that larger AAAs may remain stable or smaller AAAs may rupture [2].

The pulsatile nature of blood flow causes fluctuations in the hemodynamic forces experienced by the aorta. A consequence of such fluctuations is that arteries dilate or contract locally to maintain the value of flow-induced wall shear stress (WSS) at approximately 15 dynes/cm^2 [5], which is made possible by the ability of the endothelial cells to sense the WSS acting on them [6]. Further, arteries can also remodel themselves to a smaller or larger diameter in response to long-term changes in the WSS. Thus, it is easy to see how hemodynamic forces, and in particular the WSS, can influence the shape and size of the aorta. This has led to the widely believed hypothesis that fluctuations in the hemodynamic forces play a key role in the inception and progress of an aneurysm [5–7]. As a consequence, numerous hemodynamic parameters, most of which are based on the WSS, have been proposed that try to capture the effect of such fluctuations on the vessel wall in a single number. Some examples are the oscillatory shear index (OSI) [7], aneurysm formation index [8], and the gradient oscillatory number [9]. But a common consensus has not been reached with regard to the various hemodynamic parameters and as such, the contrasting results of various parameters further add to the confusion in their interpretation [10,11].

In vivo WSS measurement to compute hemodynamic parameters is a challenging task [12]. On the other hand, computational fluid dynamics (CFD) is a convenient method to do so and thus has been the preferred mode of investigating aneurysms. CFD simulations involve solving the Navier–Stokes equations numerically on a discretized flow domain. Since the computational cost of CFD simulations is often an issue, some simplifications in the problem setup and an optimal mesh resolution are required. Due to the pulsatile nature of blood flow, unsteady simulations are necessary, which further brings up the question of the number of cardiac cycles that should be simulated. Poelma et al. [13] showed that the typical practice of simulating five or lesser cycles is not enough for sufficient temporal convergence in the case of transitional flow.

Although hemodynamic parameters have received considerable attention, efforts have been primarily geared toward obtaining the distribution of a hemodynamic parameter over an aneurysmic surface. As such, the *underlying cause* of such a distribution and the role played by the flow field has not been widely investigated. Further, flow phenomenon, such as turbulence, has not received much attention despite the general opinion that turbulent or "disturbed flow" conditions deteriorate the arterial wall [3,14]. This study is motivated by the need to investigate and understand the underlying mechanism of flow transition to turbulence in AAAs. Since turbulent flow conditions would cause fluctuations

[1]Corresponding author.

Manuscript received December 23, 2017; final manuscript received March 23, 2019; published online April 22, 2019. Assoc. Editor: Alison Marsden.

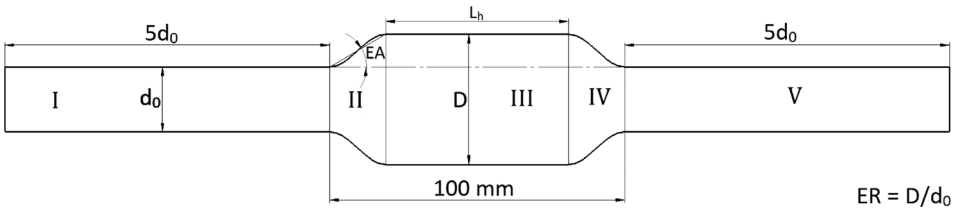

Fig. 1 General geometric aspects used to characterize a 4A geometry. Roman numerals *I–V* identify various sub parts of the geometry namely inlet, expansion region, streamwise length/ aneurysm surface, contraction region, and outlet, respectively. The inlet length and outlet length of $5d_0$ and the total aneurysm length of 100 mm are common to all the 4A geometries.

in the velocity field, regions occupied by turbulence would display high fluctuations of the velocity vector. To capture the effect of such fluctuations, the hemodynamic parameter OSI is also computed. A high OSI value is widely interpreted as a threat in the context of an aneurysm rupture [10,11,15]. The underlying hypothesis of this work is then that an AAA with a turbulent flow field could have a high OSI distribution over its surface. Further, a residence time study is also done to identify recirculation zones, which can act as a potential site for the formation of an intraluminal thrombus (ILT). The effect of turbulence on such recirculation zones is also explored.

2 Theoretical Background

2.1 Pulsatile Flow. The pulsatile nature of blood flow (see Fig. 2) greatly adds to the complexity of the flow field in an AAA. Although the flow is laminar during most phases of the cardiac cycle, at certain phases such as the peak systole, the Reynolds number (Re) is high enough for the flow to enter the transitional regime. As such, pulsatile blood flow cannot be described with the help of a single Re. Two Re are defined over the entire cardiac cycle: the mean Reynolds number Re_m (based on mean velocity v_m) and the peak Reynolds number Re_p (based on the peak velocity v_p). With ρ as blood density, μ as dynamic viscosity, and d as the diameter of the aorta, Re_m and Re_p can be formulated as

$$\mathrm{Re}_p = \frac{\rho v_p d}{\mu}, \quad \mathrm{Re}_m = \frac{\rho v_m d}{\mu} \tag{1}$$

Another dimensionless number important to characterize pulsatile flows is the Womersley number [16]. This number represents the ratio of unsteady inertial forces and viscous forces and is defined as

$$\alpha = \frac{d}{2}\sqrt{\frac{\omega}{\nu}} = d\sqrt{\frac{\pi\rho}{2\mu T}} \tag{2}$$

where ω is the angular frequency associated with the pulsatility of the flow, ν is the kinematic viscosity (μ/ρ), and T is the pulse time period. In regard to the human circulatory system, T corresponds to the time period of one cardiac cycle. At low values of α, viscous forces dominate and in the context of flow through a cylindrical geometry such as the aorta, velocity profiles resemble a parabolic profile with a time-varying maximum. But at higher values of α (>3, Ref. [17]), unsteady inertial forces start dominating that leads to a deviation from the quasi-steady parabolic profile. As heart rate and viscosity remain more or less constant, the local vessel diameter largely determines the Womersley number [18]. Maximum values are found in the aorta, in the range of 16–20 for healthy subjects at rest [6,19].

2.2 Transition to Turbulence. From a fluid dynamics perspective, blood flow in a healthy abdominal aorta is similar to an oscillating pipe flow. Since Re_m is approximately 600 in the abdominal aorta [6], the flow is expected to be laminar but at certain phases during the cardiac cycle like the peak systole, Re can be as high as 4000 in large arteries such as the abdominal aorta [6]. This is sufficiently high to trigger turbulent fluctuations.

Further, the flow field in an AAA is particularly susceptible to turbulence due to temporal deceleration and spatial deceleration. The pulsatile nature of blood flow is responsible for the temporal deceleration, whereas the geometry of the AAA is responsible for spatial deceleration. Temporal deceleration refers to the systolic deceleration or the phases right after peak systole when the flow decelerates due to a decrease in driving pressure. Such a flow deceleration destabilizes the flow field and promotes transition to turbulence [20]. Spatial deceleration can be understood by considering the flow domain geometry. Since an AAA has a larger diameter than a healthy aorta, blood has to flow through a diverging section (referred to as expansion region in Fig. 1) where it is subjected to an adverse pressure gradient that decelerates the flow and can cause flow separation. The separated shear layer can then break down due to hydrodynamic instabilities, thereby causing turbulent fluctuations. Hence, transition to turbulence can be expected in an AAA at lower than the usual thresholds for pipe flow.

3 Methods

3.1 Abdominal Aortic Aneurysms Geometry. In recent literature, a more common practice has been toward investigating patient-specific AAA cases. In this study, hypothetical axisymmetric AAA (4A) geometries are investigated for a couple of reasons. Since turbulence in AAAs has not been widely investigated, we first want to establish a general understanding of the topic. Thus, the physics observed in 4A geometries would serve as the building blocks of real AAA flow. Further, since the current clinical practice to treat AAAs is on the basis of their size, investigating 4A geometries allows for a systematic variation of the geometric parameters. This further enables the isolation of the core fluid mechanics involved, thereby allowing us to see how turbulence is affected as an AAA grows in size. Finally, the computational resources and time required to carry out a sufficiently detailed patient-specific simulation is high. Thus, a better alternative is to first establish a qualitative understanding of turbulence in 4A geometries, which will allow for a good first approximation of the flow dynamics in an actual patient-specific geometry.

A 4A geometry has two geometric parameters: the expansion ratio (ER) and the expansion angle (EA). ER refers to the ratio of the AAA diameter to the healthy aorta diameter ($d_0 = 22$ mm), whereas EA refers to the steepness of the aneurysm. Both these parameters are illustrated in Fig. 1. On average, an AAA is diagnosed at an ER of 1.5 and operated at an ER of 2.5. Thus, geometries with ER of 1.5, 2, and 2.5 are constructed. Further, 3 values of EA are considered: 15 deg, 30 deg and 45 deg. The total length of the aneurysm is kept constant at 100 mm. Various 4A geometries are referenced in this article by their ratio and angle, e.g., R2A30 implies a 4A geometry with an ER of 2 and EA of 30 deg.

3.2 Assumptions. Apart from the complexity introduced by the pulsatility of flow, the non-Newtonian behavior of blood and elasticity of the aorta further complicate blood flow dynamics in

an AAA. Numerous factors contribute to the non-Newtonian nature of blood, the most important being the dependence on the shear rate. Fortunately, the effect of non-Newtonian viscosity and elasticity on flow dynamics is secondary and can usually be neglected [6]. Thus, neglecting both these effects is a rather standard assumption in this field of study. The interested reader can find further details regarding the validity of this assumption in the specific context of the abdominal aorta in Rawat [21].

3.3 Boundary Conditions. Since the elastic nature of the aorta is ignored in this study, the usual no-slip boundary condition is applied at the aorta wall. At the outlet, gage pressure is set to zero. Such a simplified outlet boundary condition can be applied when the elasticity of the arterial wall is ignored as the flow and pressure changes due to wave reflection are no longer an issue.

At the inlet, a time-dependent velocity is prescribed to account for the pulsatile nature of blood flow. The time-dependent waveform is based on the waveform adopted by Finol and Amon [22] who constructed it on the basis of the in vivo measurements of Mills et al. [23]. In this study, the waveform is constructed based on a discrete Fourier series of 19 harmonics, details of which can be found in Rawat [21]. In accordance with the observation regarding Re_m in the abdominal aorta [6], the temporal waveform is further adapted such that $\mathrm{Re}_m = 600$. This leads to a value of nearly 3150 for Re_p and the resulting waveform is illustrated in Fig. 2. Since the heart rate is taken to be 75 beats per minute in this study, one cardiac cycle has a time period (T) of 0.8 s. On substituting appropriate values in Eq. (2), $\alpha = 16.9$ is obtained. At such a high value of α, the velocity profile displays considerable deviation from a parabolic profile and is largely flattened in the center. To achieve a good initial approximation of this deviation, a power ten spatial profile is used to represent the inlet flow in the aorta and a sufficient inlet length is provided. With the help of an inlet length development study, a length of $5d_0$ (d_0 is the healthy aorta diameter) is found to be enough for the flow to be sufficiently developed [21]. Since pipe flows usually transition at a lower Re in experiments than in numerical simulations, the inlet flow needs to be perturbed [24,25]. To do so, the velocity component perpendicular to the streamwise direction is set at 1% of the instantaneous bulk velocity in the inlet plane. This value was low enough so that it did not discernibly influence the mean flow patterns in the inlet region, but large enough to trigger instabilities in the AAA region. Tests with smaller perturbations (0.1% of the velocity) also lead to the same instabilities, but required many more cycles (>20) before their onset; this would significantly increase the computational time for the study.

3.4 Simulation Details. Three-dimensional unsteady simulations are done in ANSYS FLUENT 16.1. As explained earlier, blood is modeled as an incompressible and Newtonian fluid with a constant viscosity. The dynamic viscosity (μ) value of 0.0035 Pa·s and density (ρ) value of 1056 kg m^{-3} are adopted from the recent inter-laboratory study undertaken by the U.S. FDA [26]. The solver uses the second-order backward Euler for the temporal derivatives and the second-order central differencing scheme for the spatial derivatives.

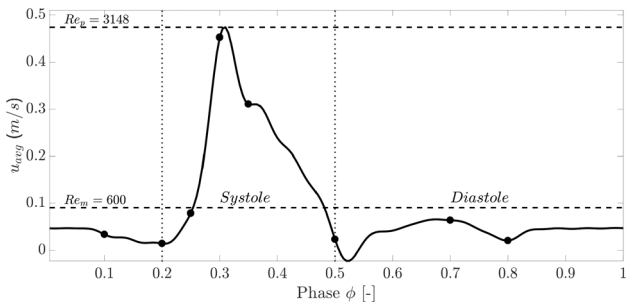

Fig. 2 Mills' time-dependent velocity waveform adapted for $\mathrm{Re}_m = 600$. The plot shows the variation of the bulk velocity against the phases of the cardiac cycle. The black markers are the phases at which data are visualized in this study. Phases 0.2–0.3 represent systolic acceleration and phases 0.35–0.5 represent systolic deceleration.

A constant time-step of 4 ms is used in simulations for all the 4A geometries. This leads to 200 time steps constituting one cardiac cycle of 800 ms. Forty internal iterations are allowed for each time-step and with the exception of a couple of phases such as the peak systole, the residual criteria of 0.001 is easily achieved within 20 time steps. Further, to ensure good outer temporal convergence, a sufficient number of cycles are simulated. Poelma et al. [13] showed how transitional flow in an AAA demands a sufficiently long time history for the computation of hemodynamic parameters. In the 4A geometries of this study, the flow generally transitions only after the first 15 cycles. Thus, the first 15 cycles are neglected from phase average calculations and the following 60 cycles are used to compute various phase-averaged quantities. Hence, visualization of any quantity at any particular phase such as $\phi = 0.5$ implies phase-averaged data over 60 cycles. It should be noted that 60 cycles is an order of magnitude higher than the number of cycles usually simulated in the majority of the existing literature. A detailed study regarding temporal convergence can be found in Rawat [21].

The 4A geometries are meshed in ANSYS ICEM CFD 16.1 using hexahedral elements. Further, the O grid blocking technique is employed throughout the flow domain so that corner elements do not suffer from face skewness, but are instead wall normal.

The average mesh element size needs to be sufficiently small to resolve the physics of the flow. However, it is difficult to predict *a priori* what the smallest length scales will be, as the only theoretical results that are available are based on homogeneous, isotropic turbulence with very large separation of scales (i.e., very high Reynolds number). Using a typical simulation, the peak dissipation rate ε [27] was evaluated. Peak values in the aneurysm region were found near $\phi = 0.1$. Dissipation rates were generally below 0.03 $\mathrm{m}^2/\mathrm{s}^3$, with a few cycles giving values up to 0.05 $\mathrm{m}^2/\mathrm{s}^3$. From these values, the smallest length scale of the flow, i.e., the Kolmogorov length scale [27], can be determined

$$\eta_K = \left(\frac{\nu^3}{\varepsilon}\right)^{1/4} \tag{3}$$

with ν the kinematic viscosity ($\nu = \mu/\rho$, here $\nu = 3.14 \times 10^{-6}$ m^2/s). For the dissipation rates mentioned earlier, we obtain values for η_K of 0.19 mm and 0.16 mm. We use an initial mesh size of $l_m = 0.4$ mm, corresponding to 2.5–3 times the Kolmogorov scale, which is generally considered to be sufficient to capture the relevant details of the flow [28]. Truly resolving the Kolmogorov length scales is not only unnecessary, but would be prohibitively expensive, especially when aiming to investigate various geometries.

Two meshes are constructed to investigate whether the grid size could be reduced: one with a general element size of l_m and the other with the general element size of 1.2 l_m. Both the meshes give similar results and thus all the 4A geometries are meshed with a general element size of 1.2 l_m [21]. This reduces the number of elements needed by nearly a factor of two, greatly reducing the computational efforts required. To capture the high gradients in the near wall region, inflation layers are employed such that the surface averaged mean y^+ is less than 1 for every 4A geometry. Such a mesh configuration results in the total number of cells ranging from 4.5 to 9.8×10^6 across all the 4A geometries. Lastly, no turbulence model is used in this study as the mesh is deemed fine enough to capture the most relevant flow scales. The choices made regarding the mesh density and the time-step size are in line with a very similar study, which included a more elaborate refinement study [13]. They are further validated by reproducing a

direct numerical simulation study of pulsatile stenotic flow [17] since the flow dynamics involved in stenotic flows are similar to the flow dynamics in an AAA. A very good agreement is observed with the direct numerical simulation results and the detailed comparison can be found in Rawat [21].

3.5 Post Processing. Post processing is done in MATLAB as it allows for convenient computation and visualization of derived quantities such as the turbulent kinetic energy (TKE)and the OSI. All components of velocity, vorticity, and WSS are exported at selected locations such as the midsectional plane and the aneurysm surface. Data export is done once every ten time steps or once every 40 ms. Thus, one cardiac cycle is visualized through 20 data files for every location of export. Only the visualization of vortex rings and associated instabilities is done in ANSYS CFD post.

The usual practice to analyze turbulent flows is to carry out the Reynolds decomposition of the relevant flow variable into a mean and fluctuating component. The purpose of doing so is to understand the contribution of the fluctuations and compare it against the mean flow contribution. Since blood flow is periodic and hence unsteady in nature, a slightly different decomposition is used to analyze such flows. This decomposition comprises a periodic and a fluctuating component [17] and for the instantaneous velocity vector **u**, it can be expressed as

$$\mathbf{u}(\mathbf{x},t) = \mathbf{u}_{\phi}(\mathbf{x},\phi) + \mathbf{u}'(\mathbf{x},t) \tag{4}$$

The first term on the RHS of Eq. (4) is the periodic or phase-averaged velocity component. It is calculated by averaging the same phases in different cycles and hence depends on position vector **x** and the phase ϕ of the cycle. The second term represents the fluctuations in the velocity field and depicts the deviation from the periodic component or what is different from cycle to cycle at the same phase. Thus, this term depicts the turbulent fluctuations. Such a decomposition can be used for other variables of interest also such as vorticity and kinetic energy.

Since the health of an AAA is what ultimately matters, it is also interesting to see the effect of turbulence on the general health of an AAA. A constant supply of fresh blood is extremely important to allow the arterial wall to absorb oxygen and stay healthy. In larger arteries, oxygen is supplied both by perfusion from the lumen and via the adventitial vaso vasorum [29]. The latter vascular system is not included in the present model, but we can investigate whether a reduced supply from the lumen will occur. A reduction in oxygen replenishment may lead to degrading the wall and increase the chances of rupture [30]. From a fluid dynamics' perspective, a stationary recirculation zone in an AAA depicts a region in which blood is constrained to vortical motion and as such, the arterial wall in the immediate local surrounding of such a recirculation zone will not be replenished with fresh oxygen from the luminal side. To identify such zones and the effect of turbulence on them, a residence time study is done. After the initial cycles, the fluid within the AAA is labeled by adding a passive scalar. An additional transport equation is then solved to keep track of this passive scalar, as it is convected by the flow.

Since popular practice in current literature is to compute hemodynamic parameters to assess the threat posed by an AAA, the OSI is also computed over the entire surface of the aneurysm. The OSI is a hemodynamic parameter that basically describes the oscillatory nature of the direction of the WSS vector and can be formulated as

$$\mathrm{OSI}(\mathbf{x}) = \frac{1}{2}\left[1 - \frac{\frac{1}{T}\left|\int_0^T \tau_w(\mathbf{x},t)dt\right|}{\frac{1}{T}\int_0^T \left|\tau_w(\mathbf{x},t)\right| dt}\right] \tag{5}$$

From Eq. (5), it can be seen that the OSI is a measure of the deviation of the local WSS vector from its mean direction. The OSI can have a value between 0 and 0.5; 0 depicting unidirectional flow and 0.5 depicting a highly oscillatory flow. High values of OSI are generally regarded to be unfavorable in relation to the health of the aorta and an AAA [6,15]. Equation (5) can be computed over multiple cycles; in this study, the OSI is computed over 60 cycles.

4 Results

4.1 Healthy Aorta Flow Dynamics. To correctly interpret the complex flow dynamics in an AAA, a baseline flow field first needs to be established and understood. To do so, blood flow through a healthy aorta is simulated. This would allow us to understand how the presence of an AAA modifies the base flow field. As expected, no turbulence is seen in a healthy aorta; the flow field is perfectly reproducible from one cycle to another. This suggests that temporal deceleration along with a small perturbation is not sufficient to trigger turbulence. It also confirms that the small perturbation applied to facilitate transition is small enough to not result in the creation of an unphysical flow field. The surface-averaged OSI is computed and found to be approximately 0.36. Considering the fact that the OSI values lie between 0 and 0.5, 0.36 is a rather high value in the context of a healthy aorta.

4.2 General Flow Field Description. In general, all the 4A geometries display a similar flow field and thus contour plots and illustrations are shown only for one particular geometry: the 4A geometry with an ER of 2 and EA of 30 deg, i.e., R2A30. Any 4A geometry that displays a different behavior is discussed separately later on in the article. In general, a vortex ring is generated at the expansion region of the 4A geometry just after the peak systole, i.e., when there is a sudden decrease in the applied inlet velocity. Figure 3 illustrates the phase-averaged z-vorticity contours at selected phases for the 4A geometry R2A30. Since the visualization is in the midsectional plane, the vortex ring is seen as a counter-rotating vortex pair between phases $\phi = 0.5 - 0.8$. The initial ring formation and advection is the same from cycle to cycle. The formation of the vortex ring is due to the roll up of the separated near-wall shear layer, wherein the initial separation is caused by the adverse pressure gradient in the aneurysm. Once formed, the vortex ring travels downstream due to its self-induced velocity and inlet bulk velocity. An azimuthal instability develops on the ring that results in the vortex core deforming in space to form a finite number of waves on the ring circumference. Once the azimuthal instability sets in, differences at the same phase between consecutive cycles start appearing. The amplitude of these waves grows as the ring advects downstream. The final breakdown of the ring into smaller vortices occurs near the distal end of the aneurysm. Depending on the geometry, the ring either breaks down into smaller vortices before it exits the aneurysm or it breaks down after hitting the contracting region near the aneurysm exit. As explained earlier in Sec. 3.5, turbulent fluctuations in the context of pulsatile flow refer to the differences at the same phase between different cycles. Since the instability growth and succeeding breakdown of the ring are not exactly reproduced from cycle to cycle, it leads to turbulent fluctuations. Thus, turbulence is locally concentrated in the spatial region where the vortex ring breaks down and the region immediately downstream. Figure 4 illustrates the turbulence intensity across all the 4A geometries at $\phi = 0.3$, as the vortex ring has undergone a complete breakdown at this phase. The intensity is calculated as the ratio of the typical velocity fluctuation $u'(=\sqrt{(2/3)TKE})$ and the bulk velocity U_{avg} at $\phi = 0.3$. The spatial concentration of turbulence can clearly be seen especially in the higher ER 4A geometries. The consequence of such localization is further explained in Secs. 4.4 and 5.2.

4.3 Residence Time. Twenty cycles are simulated to visualize recirculation regions. Figure 5 indicates the area weighted

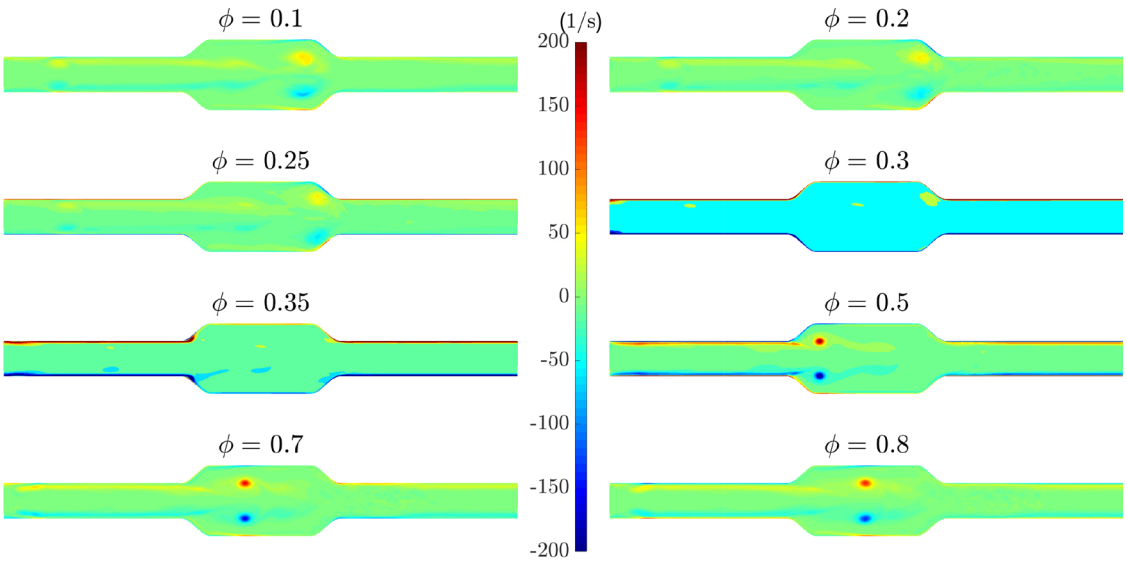

Fig. 3 Phase-averaged *z*-vorticity contours in the *XY* plane ($Z = 0$) at selected phases of the geometry R2A30. The vortex ring can be seen as a counter-rotating vortex pair in the planar contours (between $\phi = 0.5$ and $\phi = 0.8$) that breaks down near the exit region of the aneurysm. Flow is from left to right.

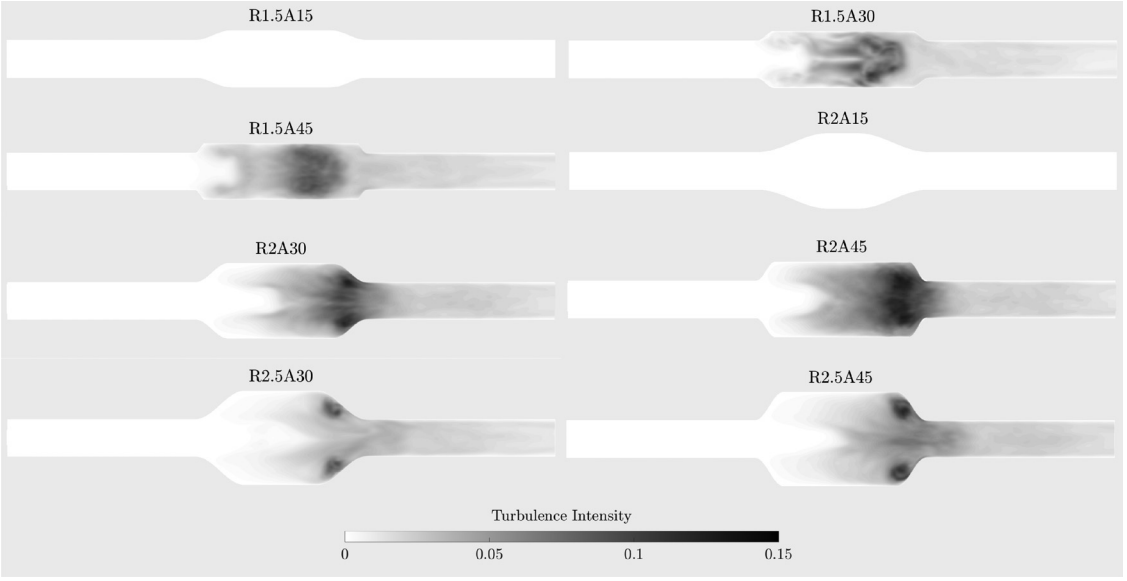

Fig. 4 Spatial distribution of turbulence intensity at $\phi = 0.3$ across all the 4A geometries. The spatial localization of turbulence is clearly visible. The 4A geometries R1.5A15 and R2A15 are free of turbulent fluctuations. Flow is from left to right.

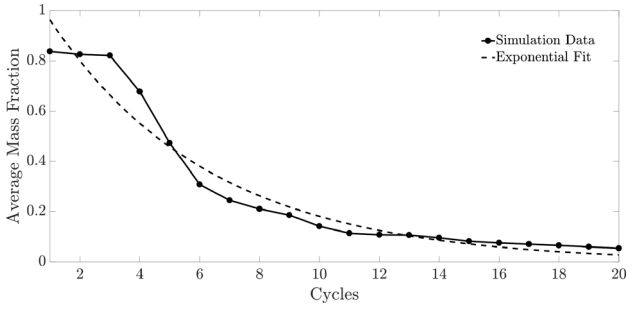

Fig. 5 Area-weighted cycle averaged mass fraction of old blood at the flow outlet of R2A30 against number of cycles simulated. Even after 20 cycles, the marked fluid has not been washed out completely from the aneurysm. An exponential fit gives a reasonable approximation of the actual plot.

cycle averaged mass fraction of "old" blood (de-oxygenated) detected at the flow domain outlet with an increasing number of cycles simulated. Old blood is computationally represented through a passive scalar in the velocity field. It can be seen that even at the end of 20 cycles, around 5% of the average mass fraction is still old blood. The trend is well approximated by an exponential curve; the curve that would have been observed in the case of a perfectly mixed flow field. However, Fig. 5 does not give an idea about the *local* concentration of old blood in the aneurysm or about the strength of a recirculation zone formed, if any. Hence, to visualize spatial regions, contour plots of the mass fraction of old blood after 4, 8, 12, 16, and 20 cycles are illustrated in Fig. 6. It should be noted that the entire flow field was seeded with the passive scalar at the beginning of 20 cycles. It can clearly be seen that even after 20 cycles the expansion region has a considerable amount of old blood (roughly 50% of the total mass fraction)

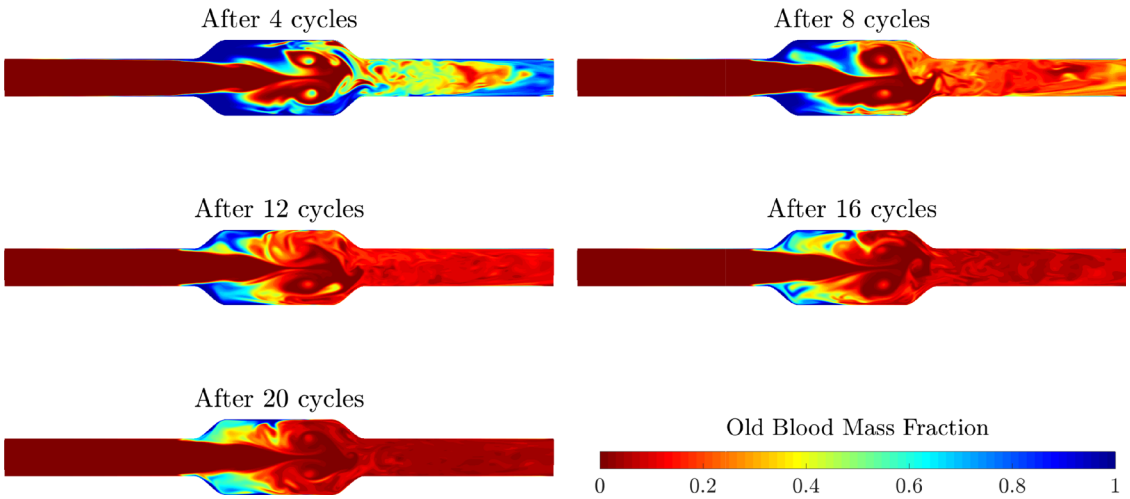

Fig. 6 Instantaneous spatial distribution of old blood mass fraction over a period of 20 cardiac cycles for the geometry R2A30. Flow is from left to right.

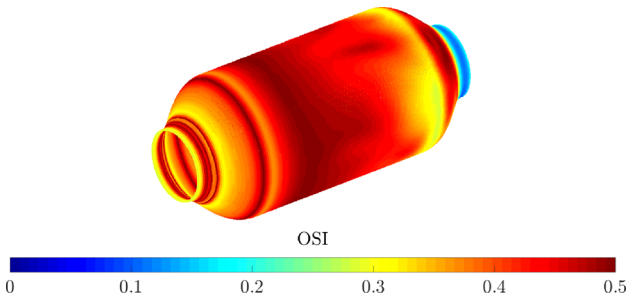

Fig. 7 Mean (over 60 cycles) OSI distribution over the aneurysm surface of R2A30. Flow is from left to right.

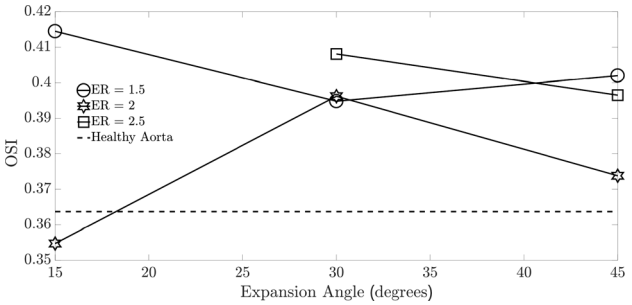

Fig. 8 Surface-averaged mean OSI of all the 4A geometries. The dashed (- - -) line indicates the average OSI for a healthy aorta.

present. But this is not reflected in the average mass fraction of old blood detected at the flow outlet, as evident in Fig. 5. Thus, from these two observations, it can be concluded that the old blood present in the expansion region of the aneurysm is stuck in a strong recirculation zone and will not leave the aneurysm until after a very long time. The location of the recirculation zones suggests that the arterial tissue will see a reduced supply from the luminal side, and must rely on the vasa vasorum (if present at the AAA location) for oxygen. The reduced oxygen supply can lead to its degradation and will expose it to a greater risk of rupture since rupture is known to be associated with wall weakening [2]. Moreover, since AAAs are often affected by an ILT [2] in the expansion region [30], our observations suggest that a recirculation zone is perhaps the predecessor to the formation of an ILT. This proposition is further discussed in Sec. 5.2.

4.4 Oscillatory Shear Index. Figure 7 illustrates the mean (over 60 cycles) OSI distribution over the 4A geometry R2A30. The OSI has a surprisingly low value at the outlet of the aneurysm, which is perhaps due to the fact that at the exit of the 4A geometry, the contraction in the cross section forces blood to exit the aneurysm, thereby ensuring that the WSS vector is more or less in the same direction at every phase of a cycle. At the beginning of this article, it was hypothesized that turbulent fluctuations could correspond to a high OSI distribution over the surface. Now, that we know that turbulence is due to the breakdown of the vortex ring and is thus spatially concentrated in the breakdown region, this hypothesis is not strictly valid across all the 4A geometries. Since the fluctuations would only affect the velocity field where the ring breaks down and the region downstream, regions upstream will not be affected. As such, turbulence will have an impact on the OSI only in the region downstream of the ring breakdown and the extent of this region varies from geometry to geometry (see Fig. 4). To compare the OSI between various geometries, the surface-averaged mean OSI of all the geometries is plotted in Fig. 8. The surface-averaged OSI of a healthy aorta is also plotted for reference. In general, all the average OSI values are within the narrow band of 0.35–0.42 and the highest ER geometries as such do not display an alarmingly high value. The highest value is observed for ER = 1.5 (R1.5A15), which would be the least worrisome case when just the diameter ratio is considered to judge the AAA. Furthermore, the lowest OSI is observed for R2A15 and in fact, it is even lower than that of a healthy aorta. This is an unexpected result since if the health of an aneurysm is to be judged on the basis of OSI, as is done in numerous studies, the healthy aorta should at least have the lowest average OSI.

5 Discussion

5.1 Structure and Stability of the Vortex Ring. Since turbulence is caused due to the breakdown of the vortex ring, it is only natural to further investigate the structure and stability of the vortex ring. Figure 9 illustrates the normalized instantaneous tangential velocity distribution across the core of the vortex ring at $\phi = 0.5$. The distribution of a Lamb Oseen (hence referred to as LO) vortex is also plotted for comparison purposes. The LO distribution is calculated by considering its circulation to be equal to that of the vortex ring. It can clearly be seen that the velocity variation is similar to the LO variation. Figure 10 further illustrates

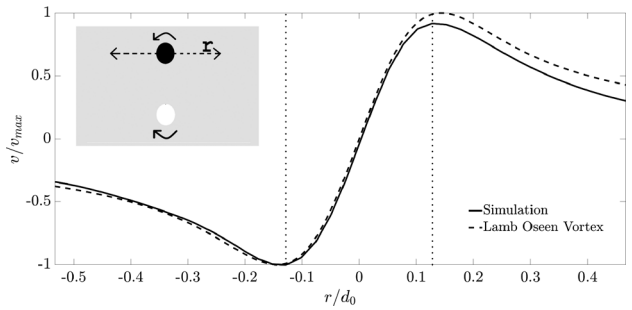

Fig. 9 Normalized *v* in the neighborhood of the core center for R2A30 at $\phi = 0.5$. The inset sketch depicts the counter rotating vortex pair and the axis along which velocity profile is plotted. The distance between the two extrema, highlighted by the two vertical dotted lines, is an indication of the vortex core diameter (*a*). The axial distance, from the center of the core ($r = 0$), is normalized with the healthy aorta diameter. From the figure, $a \approx 0.26 d_0$.

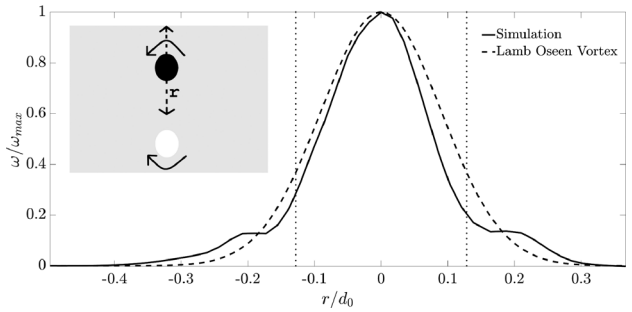

Fig. 10 Normalized *z*-vorticity (ω) distribution along the normalized distance from the center of the core for R2A30 at $\phi = 0.5$. The inset sketch depicts the counter rotating vortex pair and the axis along which *z*-vorticity profile is plotted. The vorticity peak corresponds to the core center. The vertical dotted lines indicate the core diameter as obtained from Fig. 9. From the figure, the ring radius $r \approx 0.497 d_0$, which leads to a ring diameter $d \approx 0.993 d_0$.

the similarity with a LO vortex through the normalized *z*-vorticity distribution across the vortex core. In both, Figs. 9 and 10, the LO values are a bit higher than the observed vortex core values. This is due to the fact that an LO vortex is a theoretical solution of the Navier–Stokes equations in the limit of an infinitely thin vortex core in an unconfined domain. Since the core under consideration is not thin, the ring relaxes to a new equilibrium phase during which some vorticity is lost [31]. It should be noted that such a comparison with a theoretical vortex distribution can only be done in the initial stages of the vortex ring advection as once the azimuthal instability sets in, the ring is no longer axisymmetric and segments of the ring will experience unequal influence from the other parts of the ring. Such an unequal influence causes the azimuthal instability to further grow. Interestingly, the number of waves formed on the ring circumference is not constant across all geometries. In general, the number of waves decreases with an increase in the ER: 4 waves are seen in R2A30 and R2A45 but only three in R2.5A30 and R2.5A45.

Apart from the inception and growth of the azimuthal instability, a couple of other factors are also involved in destabilizing the ring. Since the vortex ring is formed in an enclosed domain, it induces a shear layer of the opposite vorticity on the near wall. This opposite vorticity shear layer causes cross-diffusive annihilation and leads to a reduction in the ring's vorticity [32]. This is also a possible reason for the underprediction of the ring's vorticity when compared to an LO vortex having the same circulation and core radius (see Fig. 10). Further, since the azimuthal instability results in the deformation of the ring, certain parts of the ring will come in closer distance to the wall, thereby causing more intensive annihilation just on those parts. Another factor that affects the stability of the ring or rather triggers its complete breakdown is the interaction of the distorted vortex ring with the remnants of the flow field from the previous cycle. The remnant eddies are oriented in a random fashion, thus resulting in a complex vorticity field and when the distorted vortex ring, which is still a coherent vortical structure of organized vorticity, interacts with them, it completely breaks down.

The azimuthal instability is an interesting phenomenon in itself and has been the subject of numerous investigations. A detailed discussion on it is beyond the scope of this study and the interested reader is referred to the recent review by Leweke et al. [33]. However, a brief qualitative discussion is presented here. Figure 11 illustrates the growth of the azimuthal instability though an isosurface of the Q criteria [34] and colored with the streamwise (X, in this study) vorticity. The instability causes the ring to deform in space, which is clearly evident by the rearrangement of vorticity in Fig. 11. At the time of formation, the ring is perfectly circular and has no vorticity in the streamwise direction but due to the growth of the instability, vorticity rearranges itself to have a streamwise component. The azimuthal instability of a vortex ring is a combined result of Crow's instability [33] and the elliptical instability [35,36]. Crow's instability is responsible for the entire displacement of the core in space, whereas the elliptical instability deforms the core structure itself. At a later stage of the instability growth, secondary vortical structures develop on the ring and lead to the shedding of streamwise vortices in the wake [31], as depicted in subfigure (*vi*) of Fig. 11.

5.2 Flow Field Differences in Various Geometries. All the simulated 4A geometries show turbulence except two particular geometries: R1.5A15 and R2A15. A vortex ring does form in both the cases and an azimuthal instability also sets in but the amplitude of the instability does not grow enough to break the ring. Hence, the ring simply passes through the aneurysm without breaking up. Since the breakdown of the ring is responsible for turbulent fluctuations, the flow fields in these two particular geometries are completely free of turbulence. Interestingly, both the geometries have an EA of 15 deg which suggests that rings formed due to a gentler adverse pressure gradient are perhaps more stable. But the more important conclusion from this observation is that a slight change in the geometry of an aneurysm can lead to a completely different flow field. Further, the breakdown of the vortex ring is also slightly different between various 4A geometries. In geometries with the highest ER such as R2.5A30, the ring does not break until it collides with the wall of the contraction region, whereas in other cases, the ring breaks down within the aneurysm itself. The wall–ring interaction that leads to the ring breakdown is explained in detail in Rawat [21], but the important consequence of such a delayed breakdown is that turbulent fluctuations are localized to the contraction region only (see Fig. 4) and as such have little to no influence on the flow field within the aneurysm. This again highlights how small changes in the geometry can lead to considerable differences in the flow field in an aneurysm.

With respect to recirculation zones, it is seen that as the ER of a 4A geometry increases, the recirculation region increases in size. This is an expected result since a recirculation region tends to occupy the expansion region, which increases with an increase in ER. It has also been observed that the size of ILTs increases as the size of the AAA increases [37]. This further strengthens our suggestion that recirculation zones lead to the formation of an ILT. Furthermore, since recirculation zones reduce the supply of oxygen from the luminal side, bigger zones in the geometries of high ER will pose a higher threat of rupture at the expansion region. Doyle et al. [38] undertook an experimental study to highlight that from a purely mechanical perspective, the inflection (expansion

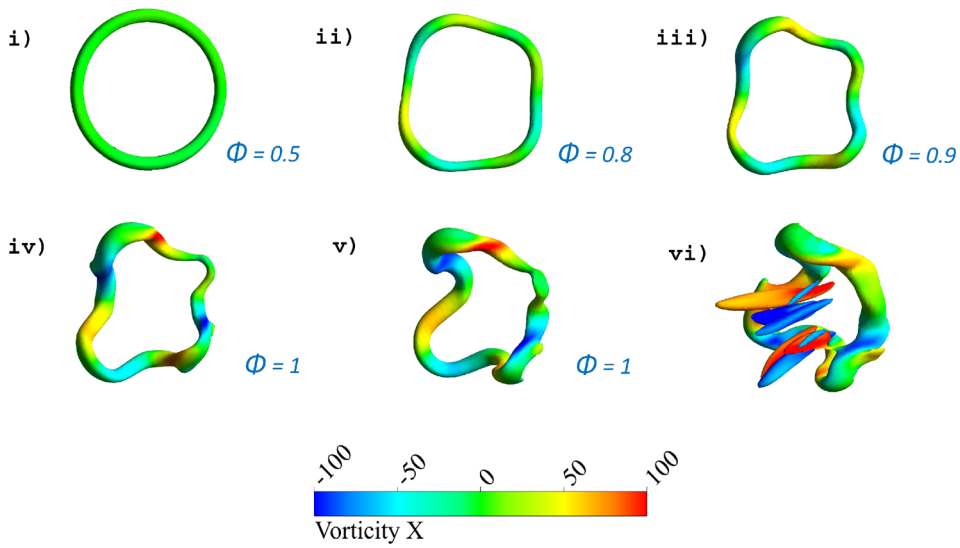

Fig. 11 Growth of the azimuthal instability on the vortex ring formed in R2A30. From (*i*)–(*v*), the rearrangement of vorticity around the ring core due to the growth of the azimuthal instability can be seen. Figure (*v*) is a 3D view at $\phi = 1$ to illustrate the large amplitude of the instability. Figure (*vi*) illustrates the core deformation and the shedding of streamwise vortices in the wake of the ring at a later stage of the instability.

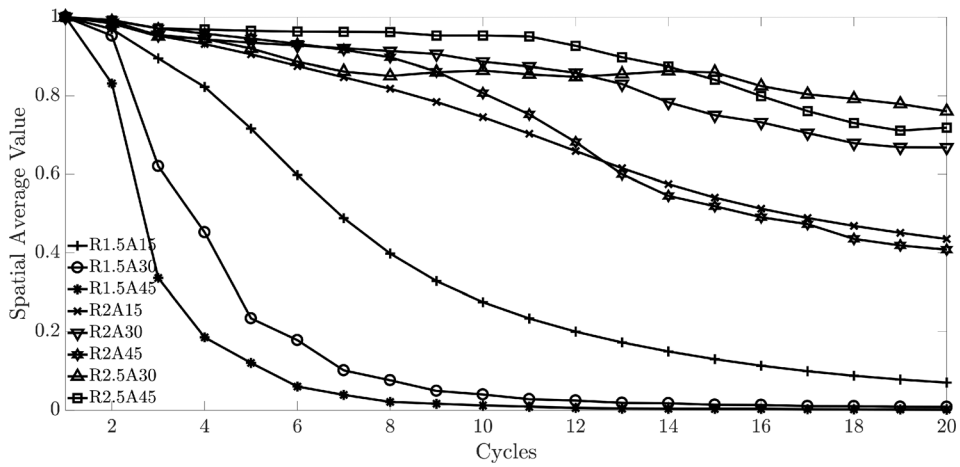

Fig. 12 Mean of area-weighted average old blood mass fraction in the expansion region with increasing number of cycles. With an increase in ER, the mass fraction of old blood stuck in a recirculation zone increases due to the size increase of the recirculation zones.

and contraction) regions are the weakest to normal hydrostatic pressure. Combining our observations with regard to recirculation zones and the observations of Doyle et al., the expansion region would be at the highest risk of rupture. This suggests that apart from hemodynamic parameters, the size of a recirculation zone should also be looked at to assess the risk posed by an aneurysm.

Figure 12 depicts the area-weighted average of old blood mass fraction at the expansion region with increasing number of cycles. As expected, for geometries with higher ER, the amount of old blood stuck in a recirculation zone increases. Even at the end of 20 cycles, the average mass fraction of old blood is nearly as high as 80% for geometries with an ER of 2.5. An interesting aspect of the plot is the significant difference between the behavior of R1.5A15 and R1.5A30/R1.5A45. Even though the ER is the same, old blood flows out of R1.5A30/R1.5A45 at a much higher rate than it does for R1.5A15. The reason for this discrepancy is turbulence. As explained earlier, turbulence is localized to the region of the ring breakdown and in geometries of ER 1.5, the ring breaks down relatively quickly as compared to other geometries, thereby causing turbulent fluctuations in the majority of the aneurysm. Thus, the enhanced mixing due to turbulence does not allow for the formation of a recirculation zone. But since there is no turbulence in R1.5A15, a recirculation region forms that greatly reduces the flushing out of old blood. On the other hand, in geometries of higher ER, the spatial region of ring breakdown is further away from the recirculation regions and thus turbulence is not able to prevent their formation. Hence, in the context of recirculation zones, depending on the geometry, turbulence can be either beneficial for an aneurysm or not have any effect.

6 Conclusions

The objective of this study was to investigate flow transition in AAAs and the underlying mechanism responsible for it. Our investigation is based on pulsatile blood flow simulations through hypothetical 4A geometries with varying ER and EA. A vortex ring is shed from the expansion region of a 4A geometry just after peak systole. The breakdown of the vortex ring into smaller vortices leads to turbulent fluctuations. Multiple factors are responsible for the ring breakdown, namely the destabilizing effect of the

arterial wall, the interaction with the remnants of the previous cycle flow field and the inception and growth of an azimuthal instability. The vortex ring did not break down in some geometries, which illustrates how minor changes in the geometry of the aneurysm can result in a completely different flow field. Further, recirculation zones were found to occupy the expansion region of the aneurysm. Such recirculation zones reduce the oxygen supply to the arterial wall from the luminal side, potentially degrading the arterial wall and increasing the chances of rupture. The size of such recirculation zones increases with an increase in the ER of an AAA. The location of such zones coincides with the location of observed ILTs, which suggests that an ILT perhaps builds up from a recirculation zone. It was seen that in some geometries, turbulence prevented the formation of such zones as it enhances mixing in the aneurysm while in other geometries it had no effect on them. Thus, it is not necessarily the case that turbulent flow has a detrimental effect on an aneurysm. Since turbulence is spatially confined to the region of ring breakdown, its impact on the OSI over the aneurysm surface depends on the geometric parameters of the aneurysm. Surface-averaged OSI for one 4A geometry was found to be lower than that for a healthy aorta, which suggests that judging the health of an aneurysm on the basis of the OSI alone is not sufficient.

A limitation of this study is that it considers smooth hypothetical axisymmetric geometries. Actual AAAs are almost never axisymmetric in shape and require a clean up to reduce the numerous local dents/kinks in their geometry before a CFD investigation can be carried out. As such, a coherent vortex ring is seldom observed in real AAAs. But formation of large vortical structures can be expected in a similar fashion as that of the vortex ring in this study. The breakdown of such large vortical structures will then lead to turbulence. The effect of turbulence on recirculation zones or a hemodynamic parameter such as the OSI will then depend on the geometry of the AAA. As such, the role played by turbulence in an actual AAA will depend on the specifics of the AAA under question but the general flow dynamics will be similar to the flow dynamics observed in this study.

Nomenclature

AAA = abdominal aortic aneurysm
CFD = computational fluid dynamics
EA = expansion angle
ER = expansion ratio
ILT = intraluminal thrombus
LO = Lamb Oseen
OSI = oscillatory shear index
TKE = turbulent kinetic energy

References

[1] Brown, L. C., and Powell, J. T., 1999, "Risk Factors for Aneurysm Rupture in Patients Kept Under Ultrasound Surveillance," Ann. Surg., **230**(3), p. 289.
[2] Vorp, D. A., 2007, "Biomechanics of Abdominal Aortic Aneurysm," J. Biomech., **40**(9), pp. 1887–1902.
[3] Lasheras, J. C., 2007, "The Biomechanics of Arterial Aneurysms," Annu. Rev. Fluid Mech., **39**(1), pp. 293–319.
[4] Kent, K. C., 2014, "Abdominal Aortic Aneurysms," New Engl. J. Med., **371**(22), pp. 2101–2108.
[5] Glagov, S., Zarins, C., Giddens, D., and Ku, D., 1988, "Hemodynamics and Atherosclerosis. Insights and Perspectives Gained From Studies of Human Arteries," Arch. Pathol. Lab. Med., **112**(10), pp. 1018–1031.
[6] Ku, D. N., 1997, "Blood Flow in Arteries," Annu. Rev. Fluid Mech., **29**(1), pp. 399–434.
[7] Ku, D. N., Giddens, D. P., Zarins, C. K., and Glagov, S., 1985, "Pulsatile Flow and Atherosclerosis in the Human Carotid Bifurcation. Positive Correlation Between Plaque Location and Low Oscillating Shear Stress," Aeterioscler., Thromb., Vasc. Biol., **5**(3), pp. 293–302.
[8] Mantha, A., Karmonik, C., Benndorf, G., Strother, C., and Metcalfe, R., 2006, "Hemodynamics in a Cerebral Artery Before and After the Formation of an Aneurysm," Am. J. Neuroradiol., **27**(5), pp. 1113–1118.
[9] Shimogonya, Y., Ishikawa, T., Imai, Y., Matsuki, N., and Yamaguchi, T., 2009, "Can Temporal Fluctuation in Spatial Wall Shear Stress Gradient Initiate a Cerebral Aneurysm? A Proposed Novel Hemodynamic Index, the Gradient Oscillatory Number (GON)," J. Biomech., **42**(4), pp. 550–554.
[10] Meng, H., Tutino, V., Xiang, J., and Siddiqui, A., 2014, "High WSS or Low WSS? Complex Interactions of Hemodynamics With Intracranial Aneurysm Initiation, Growth, and Rupture: Toward a Unifying Hypothesis," Am. J. Neuroradiol., **35**(7), pp. 1254–1262.
[11] Xiang, J., Tutino, V., Snyder, K., and Meng, H., 2014, "CFD: Computational Fluid Dynamics or Confounding Factor Dissemination? The Role of Hemodynamics in Intracranial Aneurysm Rupture Risk Assessment," Am. J. Neuroradiol., **35**(10), pp. 1849–1857.
[12] Poelma, C., Van der Mijle, R., Mari, J., Tang, M.-X., Weinberg, P., and Westerweel, J., 2012, "Ultrasound Imaging Velocimetry: Toward Reliable Wall Shear Stress Measurements," Eur. J. Mech. B/Fluids, **35**, pp. 70–75.
[13] Poelma, C., Watton, P. N., and Ventikos, Y., 2015, "Transitional Flow in Aneurysms and the Computation of Haemodynamic Parameters," J. R. Soc. Interface, **12**(105), p. 20141394.
[14] Yip, T., and Yu, S., 2001, "Cyclic Transition to Turbulence in Rigid Abdominal Aortic Aneurysm Models," Fluid Dyn. Res., **29**(2), pp. 81–113.
[15] Xiang, J., Natarajan, S. K., Tremmel, M., Ma, D., Mocco, J., Hopkins, L. N., Siddiqui, A. H., Levy, E. I., and Meng, H., 2011, "Hemodynamic–Morphologic Discriminants for Intracranial Aneurysm Rupture," Stroke, **42**(1), pp. 144–152.
[16] Womersley, J. R., 1955, "Method for the Calculation of Velocity, Rate of Flow and Viscous Drag in Arteries When the Pressure Gradient Is Known," J. Physiol., **127**(3), p. 553.
[17] Varghese, S. S., Frankel, S. H., and Fischer, P. F., 2007, "Direct Numerical Simulation of Stenotic Flows: Part 2—Pulsatile Flow," J. Fluid Mech., **582**, pp. 281–318.
[18] Poelma, C., and Hierck, B., 2015, "Hemodynamics in the Developing Cardiovascular System," *Heat Transfer and Fluid Flow in Biological Processes*, Elsevier, Amsterdam, The Netherlands, pp. 371–405.
[19] Fung, Y.-C., 2013, *Biomechanics: Circulation*, Springer Science and Business Media, Berlin.
[20] Winter, D., and Nerem, R., 1984, "Turbulence in Pulsatile Flows," Ann. Biomed. Eng., **12**(4), pp. 357–369.
[21] Rawat, D. S., 2017, "Turbulence in Aneurysms: Numerical Investigation in Abdominal Aortic Aneurysms," Master's thesis, Delft University of Technology, Delft, The Netherlands.
[22] Finol, E. A., and Amon, C. H., 2001, "Blood Flow in Abdominal Aortic Aneurysms: Pulsatile Flow Hemodynamics," ASME J. Biomech. Eng., **123**(5), pp. 474–484.
[23] Mills, C., Gabe, I., Gault, J., Mason, D., Ross, J., Braunwald, E., and Shillingford, J., 1970, "Pressure-Flow Relationships and Vascular Impedance in Man," Cardiovasc. Res., **4**(4), p. 405.
[24] Sanmiguel-Rojas, E., and Mullin, T., 2012, "Finite-Amplitude Solutions in the Flow Through a Sudden Expansion in a Circular Pipe," J. Fluid Mech., **691**, pp. 201–213.
[25] Selvam, K., Peixinho, J., and Willis, A. P., 2015, "Localised Turbulence in a Circular Pipe Flow With Gradual Expansion," J. Fluid Mech., **771**, p. R2.
[26] Stewart, S. F. C., Paterson, E. G., Burgreen, G. W., Hariharan, P., Giarra, M., Reddy, V., Day, S. W., Manning, K. B., Deutsch, S., Berman, M. R., Myers, M. R., and Malinauskas, R. A., 2012, "Assessment of CFD Performance in Simulations of an Idealized Medical Device: Results of FDA's First Computational Interlaboratory Study," Cardiovasc. Eng. Technol., **3**(2), pp. 139–160.
[27] Pope, S. B., 2000, *Turbulent Flows*, Cambridge University Press, Cambridge, UK.
[28] Moin, P., and Mahesh, K., 1998, "Direct Numerical Simulation: A Tool in Turbulence Research," Annu. Rev. Fluid Mech., **30**(1), pp. 539–578.
[29] Tanaka, H., Zaima, N., Sasaki, T., Hayasaka, T., Goto-Inoue, N., Onoue, K., Ikegami, K., Morita, Y., Yamamoto, N., Mano, Y., Sano, M., Saito, T., Sato, K., Konno, H., Setou, M., and Unno, N., 2013, "Adventitial Vasa Vasorum Arteriosclerosis in Abdominal Aortic Aneurysm," PLoS One, **8**(2), p. e57398.
[30] Vorp, D. A., Lee, P. C., Wang, D. H., Makaroun, M. S., Nemoto, E. M., Ogawa, S., and Webster, M. W., 2001, "Association of Intraluminal Thrombus in Abdominal Aortic Aneurysm With Local Hypoxia and Wall Weakening," J. Vasc. Surg., **34**(2), pp. 291–299.
[31] Archer, P., Thomas, T., and Coleman, G., 2008, "Direct Numerical Simulation of Vortex Ring Evolution From the Laminar to the Early Turbulent Regime," J. Fluid Mech., **598**, pp. 201–226.
[32] Stewart, K., Niebel, C., Jung, S., and Vlachos, P., 2012, "The Decay of Confined Vortex Rings," Exp. Fluids, **53**(1), pp. 163–171.
[33] Leweke, T., Le Dizès, S., and Williamson, C. H., 2016, "Dynamics and Instabilities of Vortex Pairs," Annu. Rev. Fluid Mech., **48**(1), pp. 507–541.
[34] Hunt, J. C., Wray, A. A., and Moin, P., 1988, "Eddies, Streams, and Convergence Zones in Turbulent Flows," National Aeronautics and Space Administration, Washington, DC, Report No. 19890015184.
[35] Widnall, S. E., Bliss, D. B., and Tsai, C.-Y., 1974, "The Instability of Short Waves on a Vortex Ring," J. Fluid Mech., **66**(01), pp. 35–47.
[36] Kerswell, R. R., 2002, "Elliptical Instability," Annu. Rev. Fluid Mech., **34**(1), pp. 83–113.
[37] Behr-Rasmussen, C., Grøndal, N., Bramsen, M., Thomsen, M., and Lindholt, J. S., 2014, "Mural Thrombus and the Progression of Abdominal Aortic Aneurysms: A Large Population-Based Prospective Cohort Study," Eur. J. Vasc. Endovascular Surg., **48**(3), pp. 301–307.
[38] Doyle, B. J., Corbett, T. J., Callanan, A., Walsh, M. T., Vorp, D. A., and McGloughlin, T. M., 2009, "An Experimental and Numerical Comparison of the Rupture Locations of an Abdominal Aortic Aneurysm," J. Endovascular Ther., **16**(3), pp. 322–335.